ELSEVIER

Journal of Contaminant Hydrology 20 (1995) 1–25

JOURNAL OF
Contaminant
Hydrology

Experimental study of movement and distribution of dense organic contaminants in heterogeneous aquifers

Tissa H. Illangasekare [a,*], James L. Ramsey, Jr. [a], Karsten H. Jensen [b], Michael B. Butts [b]

[a] *Department of Civil, Environmental and Architectural Engineering, University of Colorado, Boulder, CO 80309-0428, USA*

[b] *Institute of Hydrodynamics and Hydraulics Engineering, Technical University of Denmark, DK-2800 Lyngby, Denmark*

Received 18 October 1994; accepted 8 May 1995 after revision

Abstract

An experimental study of the migration of denser-than-water nonaqueous-phase organic contaminants through heterogeneous porous media was carried out. The purpose of the study was to observe the flow and record the migration of the contaminant to gain a fundamental insight into the way aquifer heterogeneities influence the movement and subsequent distribution of immiscible contaminants after a spill. In addition, the experiments were designed to gather quantitative data to validate multiphase flow models. The experimental results demonstrate the importance of layering in the soil in determining the flow and entrapment behavior of dense nonaqueous-phase contaminants. The findings are of use for model conceptualization and developing field characterization strategies in aquifer remediation.

1. Introduction

Effective groundwater remediation following a spill of petroleum products, hazardous waste or other industrial organic contaminants requires accurate knowledge of the subsurface distribution of the contaminant and a thorough understanding of the flow processes involved. Because these contaminants are only slightly soluble in water, they

* Corresponding author.

Elsevier Science B.V.
SSDI 0169-7722(95)00045-3

move through the soil as a separate or "immiscible" phase. As the contaminant migrates, it leaves behind a trail of immobile liquid trapped in pores between soil particles. This entrapped fluid acts as a long-term source of contamination as the immobile liquid slowly dissolves into the surrounding water.

Recent research has focused on a class of organic contaminants which are denser than water. Immiscible organic contaminants are often referred to as "nonaqueous-phase liquids", or NAPL's. Those which are denser than water are called DNAPL's. In addition to being denser than water, these liquids are sometimes volatile, and are usually highly toxic. When introduced into the subsurface, these compounds initially move downward through the unsaturated zone above the water table. If the spill is large enough and the depth to the water table is shallow, the contaminant will eventually reach the water table. Because DNAPL's are denser than water, they may continue to move downward through the saturated zone of the aquifer. However, to enter the saturated zone, the fluid must first build up adequate head to overcome the entry pressure of the water-saturated soil at the water table. Until the contaminant attains the entry pressure, it will pool up at the top of capillary fringe. Consequently, lateral spreading of the separate phase fluid is likely to occur at this location. If the lateral spreading is not too large, and enough of the spilled fluid is present at the capillary fringe to achieve the entry pressure, the contaminant will enter the saturated zone, possibly penetrating the entire thickness of the aquifer.

In natural soil formations, the movement of such contaminants is complicated by soil heterogeneities such as fractures, macropores and layering. Experimental studies by Schwille (1988), Kueper and Frind (1991), and Campbell (1992) have demonstrated that soil layering can cause lateral spreading, preferential flow paths and pooling of the organic liquid.

Schwille (1988), and Butts et al. (1993) report the initiation of unstable flow due to the presence of heterogeneities. Instabilities can cause the organic fluid to infiltrate the soil as one or more "fingers", rather than a uniform front (Held and Illangasekare, 1995a). Many researchers (Hill and Parlange, 1972; Peters and Flock, 1981; Glass et al., 1989) have proposed schemes to predict the diameter and location of such fingers. However, mainly due to small-scale heterogeneities in natural porous media, the location and diameter of the infiltrating fingers are difficult to predict.

Knowledge of the location, saturation and type of immiscible fluid within the subsurface are essential to effectively remediate a contaminated site. The use of numerical models to predict the migration of NAPL spills has been growing and gaining acceptance. Consequently, a number of multiphase flow models have been developed for contaminant hydrology applications. Multiphase flow models developed for groundwater applications include: Abriola and Pinder (1985), Faust et al. (1989), Kaluarachchi and Parker (1989), Kueper and Frind (1991), Ryan and Cohen (1991) and Al-Sheriadeh and Illangasekare (1993), among others.

Of the models which have been reported in literature, few have been properly validated. There are two primary reasons these models remain untested. First, prior to the solution developed by McWhorter and Sunada (1990), there were no analytical solutions for multiphase flow that fully incorporated the effects of capillarity. As a result, researchers have sometimes chosen to verify their models with the well-known

Buckley–Leverett solution (Buckley and Leverett, 1942) which neglects capillary gradients. Because it is well documented that capillary forces frequently dominate over applied and gravitational forces in groundwater problems, it is not appropriate to neglect capillary forces. Secondly, the controlled quantitative laboratory or field data required to validate these numerical models are not readily available. Ideally, these data should incorporate some of the complexities observed in natural soils such as heterogeneities and unstable flow of DNAPL's (Held and Illangasekare, 1995a,b).

The emphasis of this work is to provide model developers with a database of multiphase experiments for model validation. The focus of the experiments is the transport of DNAPL's in unsaturated and saturated, heterogeneous porous media. Our objectives were to record and monitor contaminant migration patterns, obtain saturation data, and to record and maintain boundary conditions during experiments.

In addition to gathering data for model validation, the experiments were designed to study closely the way heterogeneities influence the transport of dense organic contaminants. A fundamental investigation into the often competing forces of capillarity and gravity is performed through these experiments. Other items of interest include the ability of a DNAPL to penetrate the water table, the influence of the spill rate on the degree of contaminant spreading, and the organic entrapment process in both the water-saturated and unsaturated regions. This knowledge will help us to understand the behavior of DNAPL's in heterogeneous aquifers which in turn will help in site characterization and in the design and implementation of recovery and remediation schemes at contaminated sites.

2. Experimental methods and materials

Experiments were conducted in a two-dimensional soil flume equipped with a dual-gamma attenuation system to measure phase saturations. The flume was packed with three sand types to create various heterogeneous configurations. Three test chemicals were used in the spill experiments. The equipment, test materials and the experimental methods are presented.

2.1. Two-dimensional sand tank

The spill simulations were conducted in a soil flume with internal dimensions of 1.22 m × 1.83 m × 0.05 m (4 ft × 6 ft × 2 in). A schematic of the soil flume is given in Fig. 1. This flume is composed of a rigid steel frame bolted to steel end-plates. The frame and the end-plates support the front and rear walls. Steel supports are bolted to the frame, horizontally and vertically against the front and rear walls to restrict expansion when the flume is filled with soil and water. The flume walls are transparent so that the migration of the contaminant can be monitored visually during experiments. The walls are made of 1.9-cm (3/4 in) -thick Plexiglas® on the outside and lined with 0.63-cm (1/4") -thick tempered glass on the inside. The Plexiglas® supports the load exerted by the soil and water inside the flume, and the glass lining protects the Plexiglas® from the organic chemicals used in the experiment.

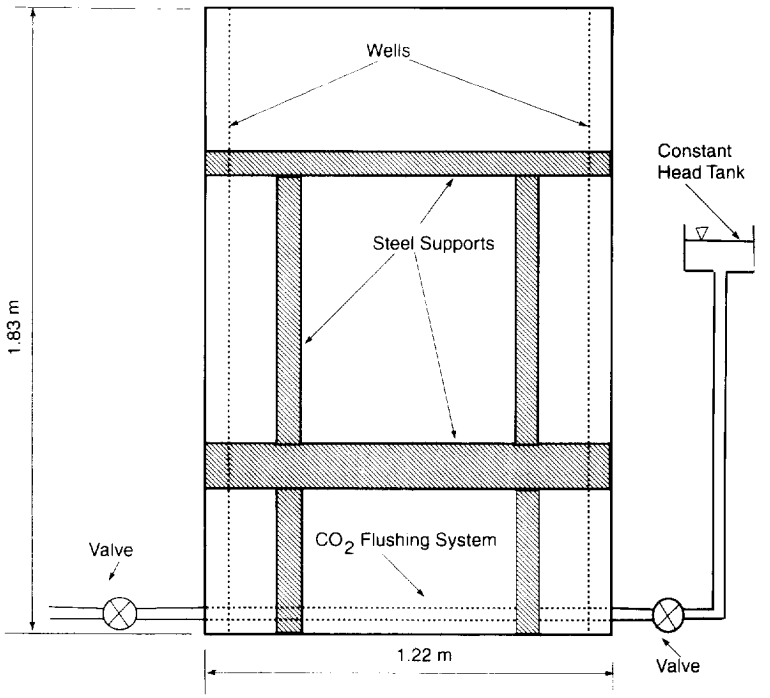

Fig. 1. Ground water flow flume.

As shown in Fig. 1, wells made of 3.8-cm (1.5 in) -diameter perforated polyvinylchloride (PVC) pipe were placed at each end of the flume. These wells were wrapped in a 125 mesh stainless-steel screens to prevent sand grains from entering the wells through perforations. The wells allow water and air to exit the flume easily during the spill. A perforated steel pipe was connected to valves at each end of the flume at its base. This system was used to flush the soil with CO_2 before saturating the soil as well as to maintain static water table conditions during experiments.

2.2. Test soils

Two or more uniform sands were used in the experiments to create a heterogeneous porous medium. Sorted silica sands obtained from crushed sandstone (GRANUSIL® silica sand by UNIMIN Corp.) were used for this purpose. The soil characteristics and the parameters of the capillary pressure saturation curves that are generally used in multiphase flow models are given in Table 1 and Table 2, respectively. The data for capillary pressure vs. saturation curves were obtained using an automated technique based on a flow pump (Manna, 1991). This technique allows for the measurement of both the drainage and wetting curves in a single experiment. Both Brooks–Corey and van Genuchten models were fitted to the data. In Table 2, S_{wr} is the residual water

Table 1
Characteristics of the sands used in the experiments

Soil type	Hydraulic conductivity (cm min^{-1})	Intrinsic permeability (m^2)	Dry bulk density (g cm^{-3})	Mean grain size (mm)	Uniformity coefficient
Sand *#16*	48.2	$9.18 \cdot 10^{-10}$	1.55	.890	1.74
Sand *#30*	11.9	$2.26 \cdot 10^{-10}$	1.60	.436	1.50
Sand *#70*	1.46	$2.78 \cdot 10^{-11}$	1.60	.198	1.86

saturation, S_m is the maximum saturation in the wetting curve, λ is the pore-index, and α and n are the van Genuchten model parameters.

2.3. Test fluids

Two denser-than-water organic fluids, namely, dibutyl phthalate (DBP) and *1,1,1*-trichloroethane (TCA), were used as the test fluids. DBP was selected as a test contaminant because its density and viscosity are similar to creosote. However, DBP is less toxic and its physical properties are far less variable than creosote, a commonly used wood preservative. Test fluid TCA was doped with *1*-iodoheptane to increase the gamma attenuation. Automate Red Dye was used to color the organics to make visual observations of the plume migration and entrapment. The relevant physical properties of the test fluids and water are given in Table 3.

2.4. Saturation measurement using dual-gamma attenuation system

During the spill experiments, the distribution of the contaminant was monitored visually using photographs and a video camera. In some of the experiments, quantitative

Table 2
Soil–water characteristics of test soils

Parameters	*#16* Sand		*#30* Sand		*#70* Sand	
S_{wr}	0.058		0.057		0.055	
S_m	0.922		0.931		0.853	
	drainage	wetting	drainage	wetting	drainage	wetting
Brooks–Corey:						
λ	2.77	2.11	3.28	2.29	2.70	1.79
P_d (Pa)	484	345	1,051	667	2,419	1,325
Van Genuchten:						
α (Pa^{-1})	0.0016	0.0023	0.00077	0.0011	0.00033	0.00060
n	5.0	3.5	5.5	4.0	4.5	3.0

Table 3
Fluid properties @ 23°C

Compound	Density ($g\ cm^{-3}$)	Viscosity (cP)	γ ($dyn\ cm^{-1}$)	
			with water	with air
DBP	1.078	11.90	21	32
TCA	1.349	1.20	26	24
Water	1.000	1.12	n.a.	71

DBP = dibutyl phthalate; TCA = *1,1,1*-trichloroethane; n.a. = not applicable.

measurements of fluid saturations were obtained using a dual-gamma attenuation system.

The gamma attenuation technique used for the measurement of phase saturations is based on the principle that different materials attenuate gamma energy by different amounts. Two sources are used to simultaneously direct γ-rays of different peak energy levels through the flume. The sources used were 50 mCi ^{137}Cs and 200 mCi ^{241}Am. Cesium-137 has a half-life of ~ 30 yr and an energy peak of 662 keV. Americium-241 has a half-life of 458 yr and an energy peak of 60 keV. By using these two energy spectra simultaneously, both the organic and the water saturations of a soil sample can be determined.

^{241}Am and ^{137}Cs γ-ray sources are mounted on a traversing gantry system near the rear wall of the flume. On the front side of the flume, a NaI scintillation photomultiplier tube detects the intensity of the γ-rays after they have penetrated through the flume and its contents. The resulting energy spectrum is processed on a microcomputer-based multi-channel analyzer (ORTEC® *918*A ADCAM).

Beer's law, originally applied to the attenuation of light, is the fundamental equation used to describe the attenuation of gamma energy. The modified form of this equation for a multiphase system of a soil with porosity ϕ, containing an organic liquid, water and air, takes the form (Illangasekare et al., 1994):

$$I = I_0 \exp - \left[\mu_s \rho_s (1 - \phi) + \mu_w \rho_w S_w \phi + \mu_o \rho_o S_o \phi \right] x \tag{1}$$

where I is the attenuated gamma intensity; I_0 is the initial gamma intensity; μ is the attenuation coefficient of the substance; ρ is the density of the substance; x is the travel distance of the γ-ray through the substance, commonly referred to as the path length; and S is the fluid saturation. The subscripts s, w and o represent the soil, water and organic phases, respectively. The attenuation due to the air phase is negligible and therefore not included in Eq. 1.

This equation can be simplified by expressing some of the variables it in terms of the bulk density ρ_b, a lumped attenuation coefficient U_i of phase i, and the volumetric phase content Φ_i of phase i, which are defined as:

$$\rho_b = \rho_s (1 - \phi) \tag{2}$$

$$U_i = \mu_i \rho_i \tag{3}$$

$$\Phi_i = S_i \phi \tag{4}$$

The simplified form of Eq. 1 is then:

$$I = I_0 \exp - [\, \mu_s \rho_b + U_w \Phi_w + U_o \Phi_o \,] x \tag{5}$$

Eq. 5 can be written for both Am and Cs sources as:

$$I_a = I_{0a} \exp - [\, \mu_{sa} \rho_b + U_{wa} \Phi_w + U_{oa} \Phi_o \,] x \tag{6}$$

$$I_c = I_{0c} \exp - [\, \mu_{sc} \rho_b + U_{wc} \Phi_w + U_{oc} \Phi_o \,] x \tag{7}$$

The subscripts a and c refer to the Am and the Cs sources, respectively.

If the bulk density of the porous medium is known, and assumed constant throughout the experiment, the attenuation due to the soil will also be constant and can be calculated as:

$$I_d = I_0 \exp - [\, \mu_s \rho_b x \,] \tag{8}$$

By substituting Eq. 8 into Eqs. 6 and 7, the two equations can be solved simultaneously for the volumetric phase contents of water and the nonaqueous fluid (Nofziger and Swartzendruber, 1974):

$$\Phi_w = \frac{U_{oa} \ln \frac{I_{dc}}{I_c} - U_{oc} \ln \frac{I_{da}}{I_a}}{(U_{wc} U_{oa} - U_{wa} U_{oc})\, x} \tag{9}$$

$$\Phi_o = \frac{U_{wc} \ln \frac{I_{da}}{I_a} - U_{wa} \ln \frac{I_{dc}}{I_c}}{(U_{wc} U_{oa} - U_{wa} U_{oc})\, x} \tag{10}$$

To use Eqs. 9 and 10, the path length and the bulk density of the soil must be known. As noted earlier, due to the internal pressure exerted on the flume walls, the flume expands when the soil is saturated. In addition to increasing the thickness of the flume, some settling of the soil also occurs which increases the bulk density. Consequently, these parameters must be determined after the soil has been saturated. Assuming the soil is completely water saturated, the following equations were developed to compute the path length and the porosity, respectively:

$$x = \frac{(U_{wa} - U_{sa}) \ln \frac{I_{0c}}{I_c} - (U_{wc} - U_{sc}) \ln \frac{I_{0a}}{I_a}}{U_{sc}(U_{wa} - U_{sa}) - U_{sa}(U_{wc} - U_{sc})} \tag{11}$$

$$\phi = \frac{U_{sc} \ln \frac{I_{0a}}{I_a} - U_{sa} \ln \frac{I_{0c}}{I_c}}{(U_{wa} - U_{sa}) \ln \frac{I_{0c}}{I_c} - (U_{wc} - U_{sc}) \ln \frac{I_{0a}}{I_a}} \tag{12}$$

The attenuation coefficients of the sand, water and TCA were determined by measuring the gamma attenuation through a known sample thickness ($\sim$ 5 cm) with a known mass of the substance in question. The gamma attenuation system was available

Table 4
Attenuation coefficients (units of $cm^2\ g^{-1}$)

Material	^{241}Am		^{137}Cs	
	mean	STD	mean	STD
Water	0.19189	0.00083	0.08816	0.00070
Sand	0.24852	0.00187	0.07844	0.00076
TCA	0.33574	0.00181	0.07813	0.00133

STD = standard deviation; TCA = *1,1,1*-trichloroethane.

only for the TCA experiments. The attenuation coefficients for TCA, sand and water were computed by reformulating Eq. 1. The values used in this study are given in Table 4.

2.5. Spill procedure

The chemical spills were performed using a fluid delivery system attached to a line source injector. In experiments that required a constant head, the head at the injection point was maintained by pumping the test fluid from a reservoir to a constant-head tank connected to the injector. The mass of fluid in the reservoir was recorded continuously during the experiment by placing the reservoir on an electronic balance interfaced to a computer. In experiments that required specified flux conditions, a pump was used to deliver the fluid at a constant rate. The injection device was made of aluminum and was designed to allow the organic to contact the soil in a 4.45 cm (1 3/4 in) by 0.32 cm (1/8 in) area. The injection port was oriented with its long side perpendicular to the flume walls. This configuration created a line source in three dimensions or a point source in two dimensions.

3. Experiments and results

Once assembled, the flume was packed with unconsolidated sands in various configurations. The soil configuration, boundary conditions, injection conditions and the contaminant used were changed from one experiment to the next. This was done in part to look at different aspects of the problem and also to improve the quality of the data of subsequent experiments. For instance, during the first two experiments, DBP was used as the contaminant. In the remaining experiments TCA was used. The reason for the change was we wished to observe DNAPL transport in the saturated zone. Because DBP is only slightly denser than water, substantial buildup of DBP on top of the capillary fringe is required for it to attain the entry pressure of the soil and move into the saturated zone. TCA, on the other hand, is far more dense than DBP and was therefore far more likely to penetrate into the saturated zone.

In all unsaturated-zone spill experiments, the flume was 1.22 m (4 ft) wide by 1.83 m (6 ft) high, as shown in Fig. 1. In the first saturated-zone experiment, the organic was found to spread to the end-plates of the flume. Hence to avoid this boundary effect, in

Table 5
Summary of the experimental conditions

Experiment No.	Water saturation in soil before spill	Organic test fluid	Heterogeneous sand packing
1	unsaturated	DBP	*#16* lens in *#30* matrix
2	unsaturated	DBP	*#70* lens in *#30* matrix
3	unsaturated	TCA	5-cm alternate layers of *#30* and *#70*
4	unsaturated	TCA	20-cm alternate layers of *#30* and *#70*
5	saturated	TCA	single 20-cm layer of *#70* in *#30* matrix
6	saturated	TCA	single 20-cm layer of *#16* in *#30* matrix

DBP = dibutyl phthalate; TCA = *1,1,1*-trichloroethane.

the second saturated-zone experiment, the flume was rotated 90° to make the dimensions 1.83 m (6 ft) wide by 1.22 (4 ft) high. By making the width of the flume 1.83 m, the contaminant could spread further before it encountered the end-plates of the flume.

Six experiments with various soil packing configurations and under saturated and unsaturated soil conditions were conducted. The experimental conditions are summarized in Table 5. Gamma scanning was used in experiments *4–6* to determine the fluid saturations. As the gamma system was not available for experiments *1–3*, the plume location was tracked visually.

After completing the analysis of both the DBP experiments, we determined that the saturation measurements made with dual-gamma system were very sensitive to the path length of the gamma beam and hence to the internal thickness of the flume. When the flume is packed with soil and then filled with water it expands in an non-uniform manner. As a result, the internal thickness of the flume varies at each location. The dual gamma system can be used to determine the thickness if it can be assumed that the soil is completely water saturated. In the later experiments where TCA was used, to completely saturate the soil, the air inside the flume was displaced with CO_2 for 6 h after packing the dry sand. CO_2 was selected to displace the air because it is denser and much more soluble in water than air. After removing the air, the flume was slowly filled with degassed distilled water. The flume was then left undisturbed so that any entrapped CO_2 would dissolve into the water. After 24 h, a hydraulic gradient was applied across the flume using the wells at both ends. Water containing dissolved CO_2 was removed from the flume and replaced with fresh degassed distilled water for an additional 24-h period. After scanning the saturated flume to determine the thickness and the bulk density distributions, the water level was slowly lowered to 90 cm above the base of the flume. A constant head was established at the base of the flume by connecting the perforated PVC pipe used to flush the soil with CO_2 to a constant-head tank. The flume was then left undisturbed for 7 days to reach equilibrium.

*3.1. Dibutyl phthalate (*DBP*) in unsaturated soil*

The purpose of the first two unsaturated-zone experiments (experiments *1* and *2*) was to compare the migration pattern of an organic in a heterogeneous soil with that in a

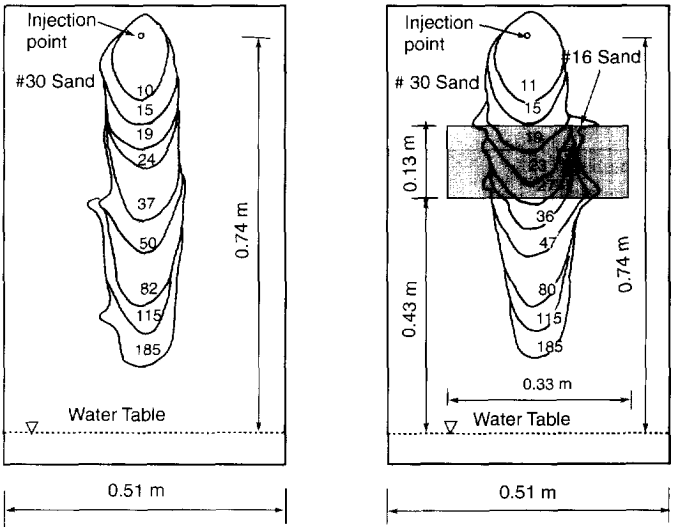

Fig. 2. DBP migration through a coarse lens in unsaturated soil (the *numbers* shown on the *contour lines* are the observation times in minutes after the spill).

homogeneous soil. The flume was divided into two vertical halves with a perforated PVC pipe. The left-hand half of the flume was packed homogeneously with *#30* sand. On the right-hand half, that was also dry packed with *#30* sand, a small lens of a different sand was placed to create a simple heterogeneity. In experiment *1*, the lens

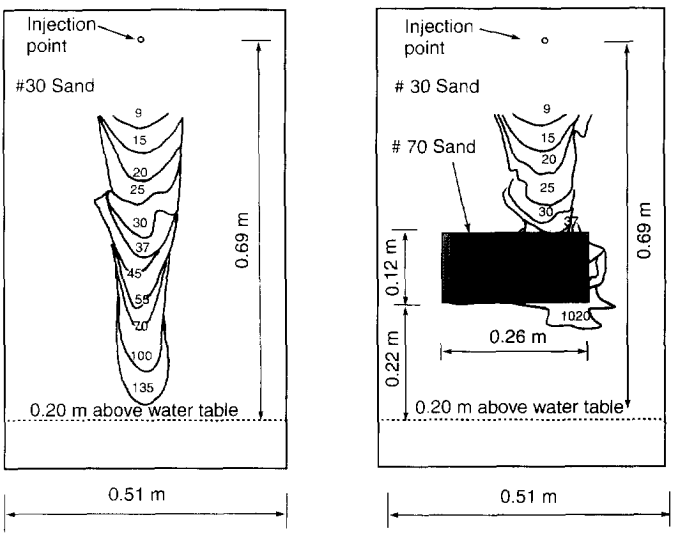

Fig. 3. DBP migration through a fine lens in unsaturated soil (the *numbers* shown on the *contour lines* are the observation times in minutes after the spill).

consisted of a coarse soil, sand *#16*. In experiment *2* the lens was made with a fine soil, sand *#70*. After packing, the flume was saturated from the bottom up and then de-saturated and allowed to equilibrate with the water table. The water table was maintained with a constant-head tank apparatus in the lower portion of the flume, below the lens. The relative position of the water table to the injection point and the size and location of the lenses for experiments *1* and *2* are presented in Fig. 2 and Fig. 3, respectively.

A constant flux spill condition was used in both these experiments. A DBP fluid volume of 500 mL was simultaneous injected as a point source into the left-and right-hand side of the flume at a constant rate of 33 mL min^{-1}.

3.1.1. Experiment 1: coarse lens in unsaturated soil

In Fig. 2, the migration patterns of DBP through the homogeneous soil and the soil containing the coarse lens are compared. The contour lines in this figure represent the position of the advancing front observed visually through the walls of the flume as a function of time (in minutes). These observed fluid front profiles show that the presence of the coarse lens had virtually no influence on the transport of the organic. Quite interestingly though, some spreading of the DBP was observed at both the top and bottom interfaces of the lens.

3.1.2. Experiment 2: fine lens in unsaturated soil

Unlike the previous experiment, the fine lens substantially altered the migration of the organic. The position of the advancing front of the DBP as a function of time is shown in Fig. 3. At the instant the DBP contacted the fine lens, it rapidly entered the lens and began to spread laterally as well as vertically. Clearly, capillary forces were pulling the organic into the fine sand lens.

In these two experiments, the fine lens entrapped the majority of the organic preventing it from reaching the capillary fringe. Except for some entrapment at the soil interfaces, the coarse lens had virtually no impact on the contaminants migration. No evidence of unstable flow was observed during either of these experiments.

*3.2. 1,1,1-Trichloroethane (*TCA*) in unsaturated soils*

These two experiments were performed to observe the transport of a chlorinated solvent in a multi-layered system. During packing, the sand was tamped down every 5 cm to maintain a consistent and tight pack. Soil packing was performed by pouring dry sand through a PVC pipe. The pipe contained two metal screens that rotated the grains and allowed the sand to drop at a uniform velocity, resulting in a uniform packing. Two sets of screens were used in the packing process, one for the *#30* sand and finer screens for the *#70* sand.

3.2.1. Experiment 3: 5-cm-thick layered packing

The point of spill was located on the vertical center line of the plume at a depth of 12 cm below the soil surface. A total mass of 2000 g of the fluid was injected during a

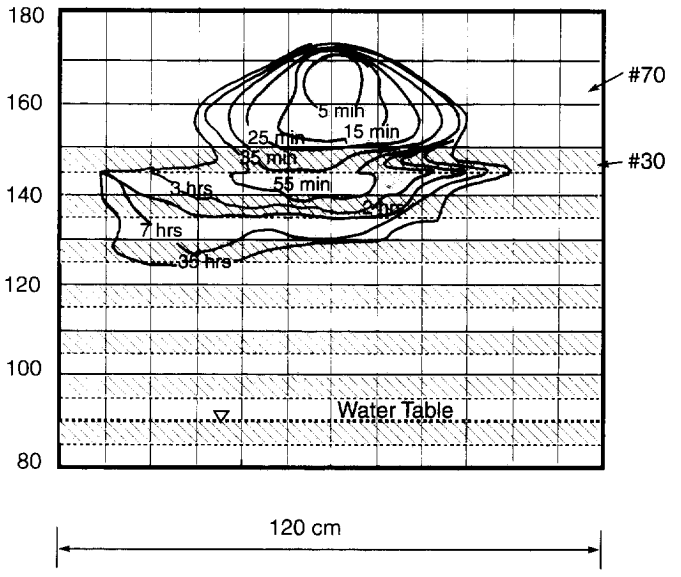

Fig. 4. Migration pattern: 5-cm-layer unsaturated-zone TCA experiment (elevations in cm above tank base).

40-min period at a mean rate of 37 mL min^{-1}. The exact flux rates as recorded using the electronic balance for all experiments including this are given in Ramsey (1992).

Under static conditions, in the layered soil, the initial water saturation changed with the elevation as determined by the capillary pressure vs. saturation curve of each soil. The influence of the initial water saturation profile on the TCA migration pattern can be seen in Fig. 4, where the position of the advancing front is plotted. At the beginning of the spill, the organic's initial movement was predominantly vertically downward. After only a couple of minutes, capillary forces in the *#70* sand quickly spread the contaminant laterally as well as vertically. In 25 min, the TCA had reached the first coarse layer. At this time, the width of the plume was approximately equivalent to its vertical penetration, indicating that capillary forces controlled the TCA migration through the first fine layer.

The initial water saturation in the first coarse layer was lower than the water saturation in the fine soil above. As a result, for the two soils used, the relative permeability to the organic phase was greater in the coarse layer than in the fine layer above or below. Also, the intrinsic permeability of the *#30* sand is an order of magnitude greater than the *#70* sand (Table 1). These two factors in combination make the effective permeability to the organic phase much higher in the coarse layer than in the fine layer. Consequently, movement through the coarse layers is controlled by gravitational forces with little or no spreading due to capillary forces.

Upon reaching the next fine layer, the capillary forces of the fine soil pulled the TCA into the fine layer. The contour line of 55 min in Fig. 4 illustrates this observation. The effective permeability of the coarse soil is much greater than the effective permeability of the fine soil. Hence, the fine layer does not have the capacity to transmit all the oil

that infiltrated through the coarse layer, resulting in the TCA ponding up at the base of the first coarse layer. The ponding of the organic led to the development of horizontal gradients which caused the TCA to spread horizontally along the base of the coarse layer. This spreading continued for a little over 3 h.

Quite interestingly, subsequent migration was mostly vertical. It appears that the amount of horizontal spreading was controlled by the effective permeability of the first coarse layer and the underlying fine layer. The implication of this observation is that if one can determine the degree of spreading based on the physical properties of the first coarse layer and the underlying fine layer, subsequent transport quite possibly could be modeled as one-dimensional flow.

As in the DBP fine lens experiment, capillary entrapment prevented the TCA from reaching the fully saturated soil. Based on the color intensity of the video recording, it can be concluded that a majority of the TCA remained within the fine layers due to capillary effects.

3.2.2. Experiment 4: 20-cm-thick layered packing

Saturation profiles were obtained during the spill at three different times using the dual-gamma system. Saturation data were obtained at 1-cm intervals, beginning 10 cm below the injection point and extending vertically beyond the migration of the TCA.

In the previous experiment, the TCA injection took place in the *#70* sand. In this experiment, the TCA was injected into the coarser *#30* sand. The point of injection was located on the vertical center line of the tank at a depth of 12 cm from the soil surface. The same head was applied to the TCA at the injection device in both experiments. Because the permeability of the *#30* sand is much greater than the permeability of the *#70* sand, the injection rate in the second experiment is much greater than the injection

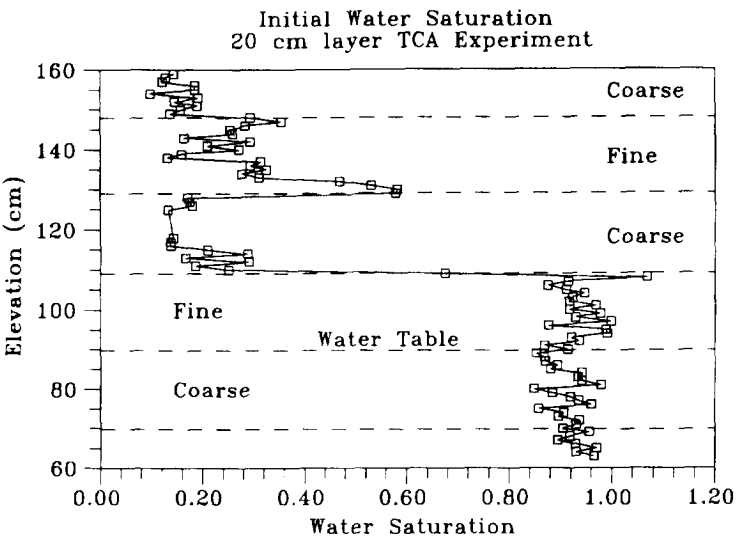

Fig. 5. Initial water saturation for 20-cm-layer TCA spill.

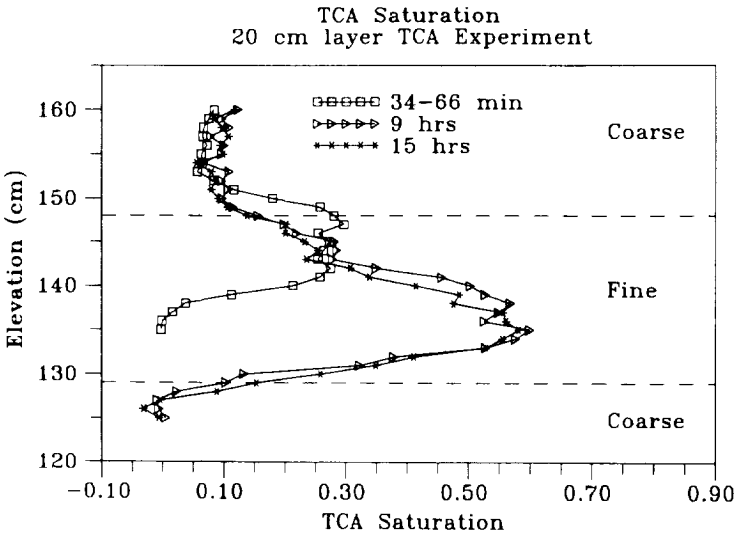

Fig. 6. TCA saturation 20-cm-layer TCA spill.

rate of the first experiment. A total mass of 4600 g was injected during a 10-min period at an average rate of 340 mL min^{-1}.

The initial water saturation profile measured using the gamma system is given in Fig. 5. The saturation profiles and the two-dimensional migration pattern of the TCA are

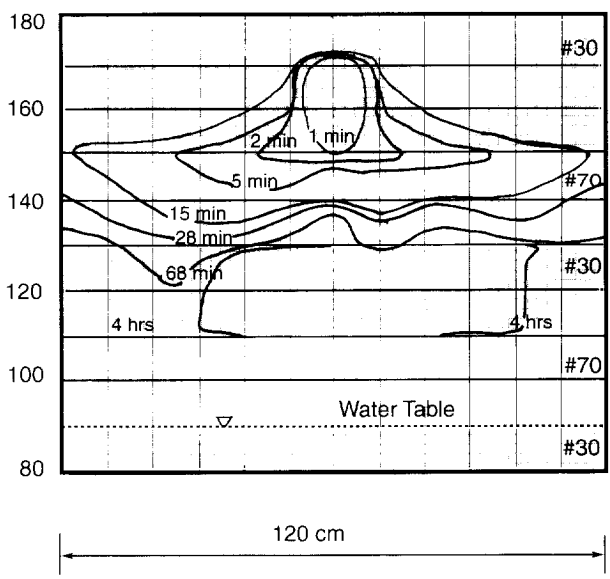

Fig. 7. Migration pattern: 20-cm-layer unsaturated-zone TCA spill (elevations in cm above tank base).

shown in Fig. 6 and Fig. 7, respectively. Initially the TCA moved vertically downward. Upon contacting the first fine layer, the plume moved laterally through the coarse layer. This response is similar to what was observed in the previous experiment, where the first coarse layer was overlying a fine layer. However, because the injection rate of this experiment was much greater than the previous experiment, the head gradient in the coarse layer was also greater. As a result, the TCA spread at the base of the coarse layer much faster than it could penetrate the fine layer. After only 15 min, the organic had reached the end of the flume and began entering the wells at the boundary.

The saturation profiles provide some useful insight into the migration pattern presented in Fig. 7. Notice that the TCA had difficulty moving into the first *#70* layer directly beneath the injection point during the initial stages of the experiment. This can be explained by first noticing the initial water saturations at the top and bottom of this layer (shown in Fig. 5) are greater than the water saturation in the middle of the layer. The high water saturation in the bottom of the layer corresponds closely with the static capillary pressure–saturation curve of the *#70* sand. The high water saturation at the top of the layer indicates a barrier effect at the interface between the *#30* and *#70* layers (Walser et al., 1994).

The first saturation measurements made during the spill were completed well after the injection was discontinued and the TCA had already spread to wells at both ends of the flume. Quite interestingly, the infiltrating TCA saturation was initially relatively low at only ~ 28% in the fine sand. This occurred because the bulk of the organic bypassed this location due to its high initial water saturation and hence low relative permeability of organic, relative to other locations along the top of the *#70* layer. This can be seen in Fig. 7, as the organic moves predominately through the left-hand side of the flume.

At later times, the TCA is shown ponding on top of the capillary fringe at the base of the *#70* sand layer. Much higher organic saturations were observed at these times. Most likely, the TCA moved into the center of the flume from the sides. The TCA did penetrate into the coarse layer below, but primarily near the ends of the flume. One possible explanation is that the presence of the wells at the ends of the flume permitted the water to evaporate which in turn made penetration by the TCA easier.

3.3. 1,1,1-Trichloroethane (TCA) in saturated soil

In these experiments, the flume was rotated 90° to allow the TCA to spread further laterally before encountering the end-plates. A single 20-cm layer was positioned in an otherwise homogeneous *#30* sand matrix. A schematic of the soil configuration used in these experiments is shown in Fig. 8.

In the first experiment, a fine sand, *#70*, was used to create the layer. In the second experiment, a coarse sand, *#16*, was used. The bottom of the layer was placed 40 cm above the base of the flume, therefore, the top of the layer was 60 cm above the base. TCA was injected at a point 100 cm above the base.

3.3.1. Experiment 5: single fine layer

Prior to the spill, dual-gamma scans of the saturated soil were used to determine the dry bulk density and the thickness, or path length of the flume. In both experiments, a

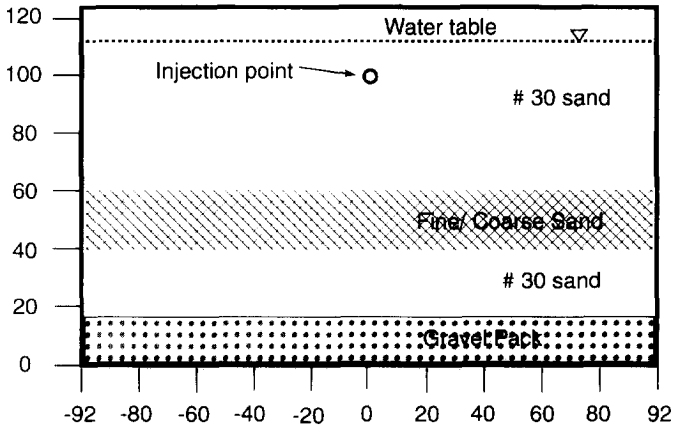

Fig. 8. Soil configuration for saturated-zone TCA spill experiment.

vertical profile was measured every 2 cm beginning directly below the injection point. The dry bulk density of the sand in the first experiment varied from ~ 1.35 to ~ 1.55 g cm^{-3}. A total fluid mass of 3600 g was injected during 45-min period at an average rate of 59 mL min^{-1}.

Saturation profiles along the vertical center line of the flume are presented in Figs. 9–11. Each data point was measured with a 60-s "live time". The actual amount of time it takes to acquire an individual data point is greater than the "live time" by the amount of detector "dead time" and the computational overhead. For a detailed discussion of live and dead time, the reader is referred to Nofziger and Swartzendruber (1974). The actual time required to obtain the data presented here was ~ 90 s per data point. The times shown in Figs. 9–11, represents the interval over which the data profile was acquired and are relative to the time the injection began.

Due to the driving head at the point of injection, the TCA initially spread in all directions. Because the density difference between the water and the DNAPL is significant, the movement of the organic plume was mostly vertically downward through the *#30* sand. Two sample photographs from a series taken in this experiments is given in Fig. 12a and b. Fig. 12a shows the influence of the density gradient, 15 min after the beginning of the spill. Fig. 12b shows 15 h after the spill, how the fine layer is acting as a barrier to the fluid and the lateral spreading at the interface of the two soils. Captions are provided in Fig. 12c and d to identify the injection points, soil types and notable features of the plumes.

The saturation data in Fig. 9 are at the time the TCA had moved through the coarse layer and just encountered the fine layer below. The maximum organic saturation in the coarse layer was ~ 75%. There was no indication that the TCA was able to penetrate into the fine layer during this period.

Fig. 10 shows the TCA position and saturation well after the injection had been discontinued. The shape of the "receding front " and the residual TCA saturation can be determined from Fig. 10. Unable to penetrate the fine layer, the TCA began build up

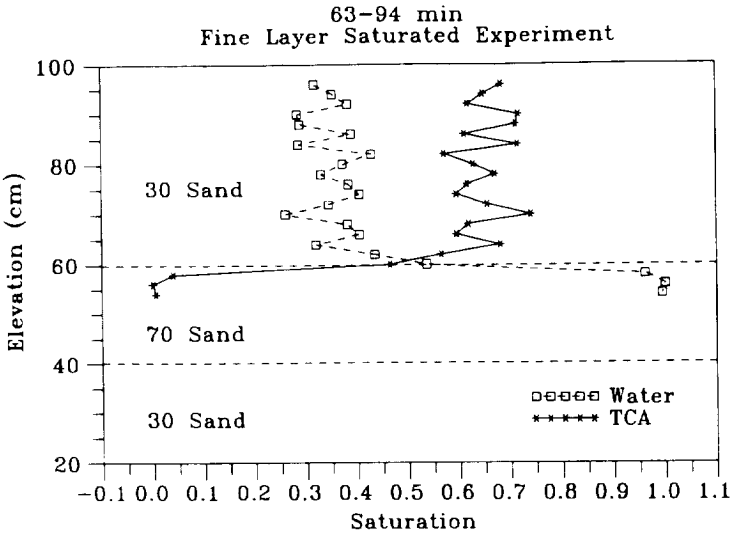

Fig. 9. Fine-layer saturated experiments: 63–94 min after spill.

at the layer interface. As in the previous experiments, this led to spreading at the base of the coarse layer. However, in this case the fine layer acted as a barrier and the fluid did not penetrate into the fine layer as a front.

Spreading of the contaminant continued but at a much slower rate than during the first 3 h after the injection. The saturation data of Fig. 11 clearly show the TCA

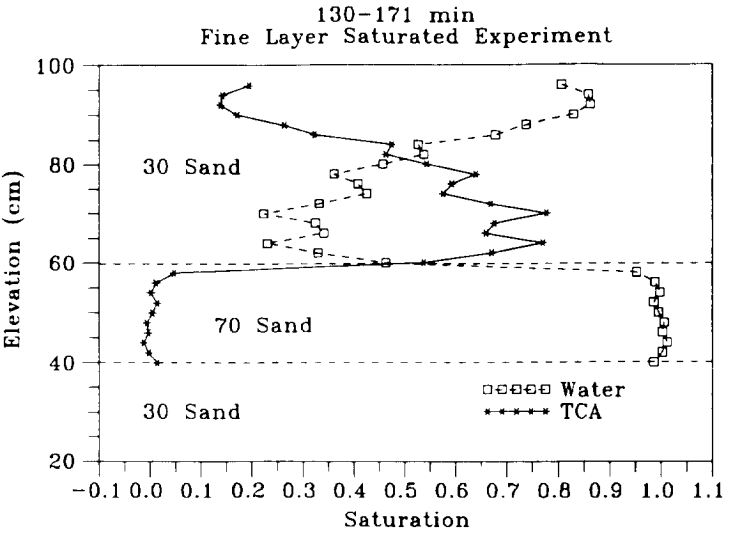

Fig. 10. Fine-layer saturated experiments: 130–171 min after spill.

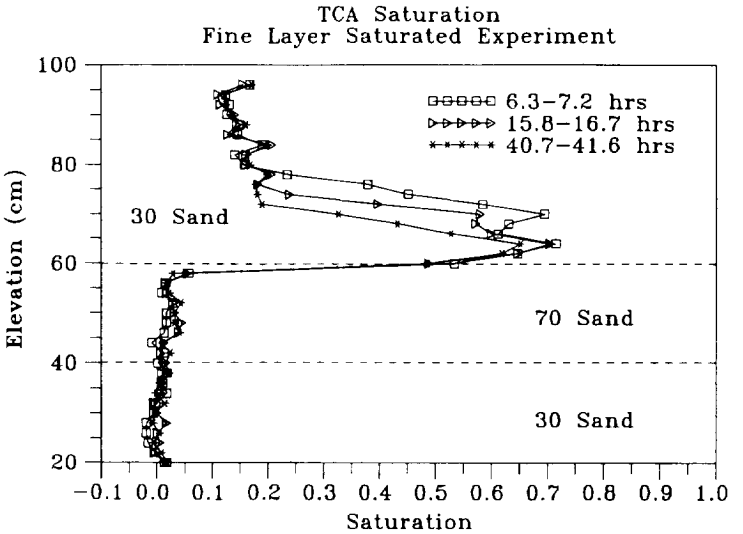

Fig. 11. Fine-layer saturated experiments, profiles from 6.3 to 41.6 h.

continued to drain from the coarse layer. Since the organic had practically ceased lateral spreading, but continued to migrate from the coarse layer it must have been moving through the fine layer as single or multiple fingers. Indeed, Fig. 12b (also identified in Fig. 12d) shows a finger developing in the *#30* sand layer beneath the *#70* sand layer. The fingers are not visible in the *#70* sand layer because they are believed to be much smaller than the thickness of the flume.

It is unknown when the instability developed, or the number, size, or frequency of the fingers that resulted. It appears the presence of the fine layer contributed to the initiation of the instability by spreading the contaminant along the top of the layer. Unable to achieve the entry pressure required to penetrate the fine layer, the organic began channeling through the largest pores spaces available. Even though substantial effort was put into creating homogeneous layers, local heterogeneities within the layers themselves also contributed to the instability.

Although this experiment was not designed to look at the details of the fingering process, it does appear that the fingers developed in this experiment were very small. This observation supports the work of Stokes et al. (1986), who suggested that the unstable displacement of a wetting phase by a non-wetting phase would result in fingers of width comparable to the characteristic pore size.

3.3.2. Experiment 6: coarse layer

This experiment was set up identical to the previous experiment except that the fine *#70* sand layer was replaced with a coarse *#16* sand layer. The location of the layers, the injection point, and the position of the water table relative to the base of the flume are presented in Fig. 8. A total fluid mass of 3900 g was injected during a 68-min period at an average rate of 43 mL min^{-1}.

The transport of the organic during the initial stages of the experiment was essentially identical to what occurred in the first experiment, only slower due to the reduced injection rate. Two photographs from a series that was taken during the spill are shown in Fig. 13a and b. The initial migration pattern can be seen in Fig. 13a, taken 30 min after the beginning of the injection. Once again gravitational forces due the density difference between water and TCA moved the organic predominately downward. Fig. 13c identifies the notable features of the plume shown in Fig. 13a.

Shortly after stopping the TCA injection, very little movement of the organic at the infiltrating front could be seen through the flume walls. Approximately 110 min into the spill, TCA fingers were seen developing in the *#16* sand coarse layer.

Clearly, the lack of stable displacement at the infiltrating front was because the organic became unstable and began to finger through both the *#30* and *#16* sand below. The instability is believed to have been triggered by the removal of the applied head when the injection was discontinued. After a short period of time, the applied force was dissipated as the TCA continued to migrate downward. It appears that gravitational forces alone were insufficient to maintain a stable displacement. Consequently, the TCA began to channel or finger through the largest available pore spaces.

After fingering through the *#16* sand layer, the TCA was initially unable to achieve the entry pressure of the *#30* sand and continue its downward migration. As a result, the organic began to pond on top of the *#30* sand. Ponding led to the development of pressure gradients in the organic phase and subsequent stable flow in the form of spreading along the base of the coarse layer. This is shown in Fig. 13b that was taken 2 h after the spill. The notable features of the plume are identified in Fig. 13d. Ponding also raised the pressure of the organic to the entry pressure of the *#30* sand. This initiated unstable flow in the *#30* sand and the gravel pack below.

The first saturation data acquired in this experiment, captured the saturation profile at the infiltrating edge of the organic, or the "front". This data illustrate the sharpness of the saturation profile at the front. The scan was started while TCA was still being injected into the flume, and is presented in Fig. 14. The measured saturation during this scan and was 81%, which is slightly greater than the maximum saturation of 75% measured in the previous experiment.

Fig. 15 and Fig. 16 present the saturation profile after the TCA began to pond and spread at the base of the coarse layer. The organic is shown moving from the *#30* sand in upper portion of the flume and ponding at the base of the #16 layer. Indications of fingering through the coarse layer and the *#30* sand below the coarse layer can also be seen in these figures.

The fingers developed in this experiment were much smaller than the thickness of the flume or the resolution to be captured by the dual-gamma system. Consequently, the

Fig. 12. Photographs of:
a. Fine-layer experiment, 15 min after spill.
b. Fine-layer experiment, 15 h after spill.
Ibidem, with captions:
c. Plume configuration, 15 min after the spill in the fine-layer experiment.
d. Plume configuration, 15 min after the spill in the fine-layer experiment.

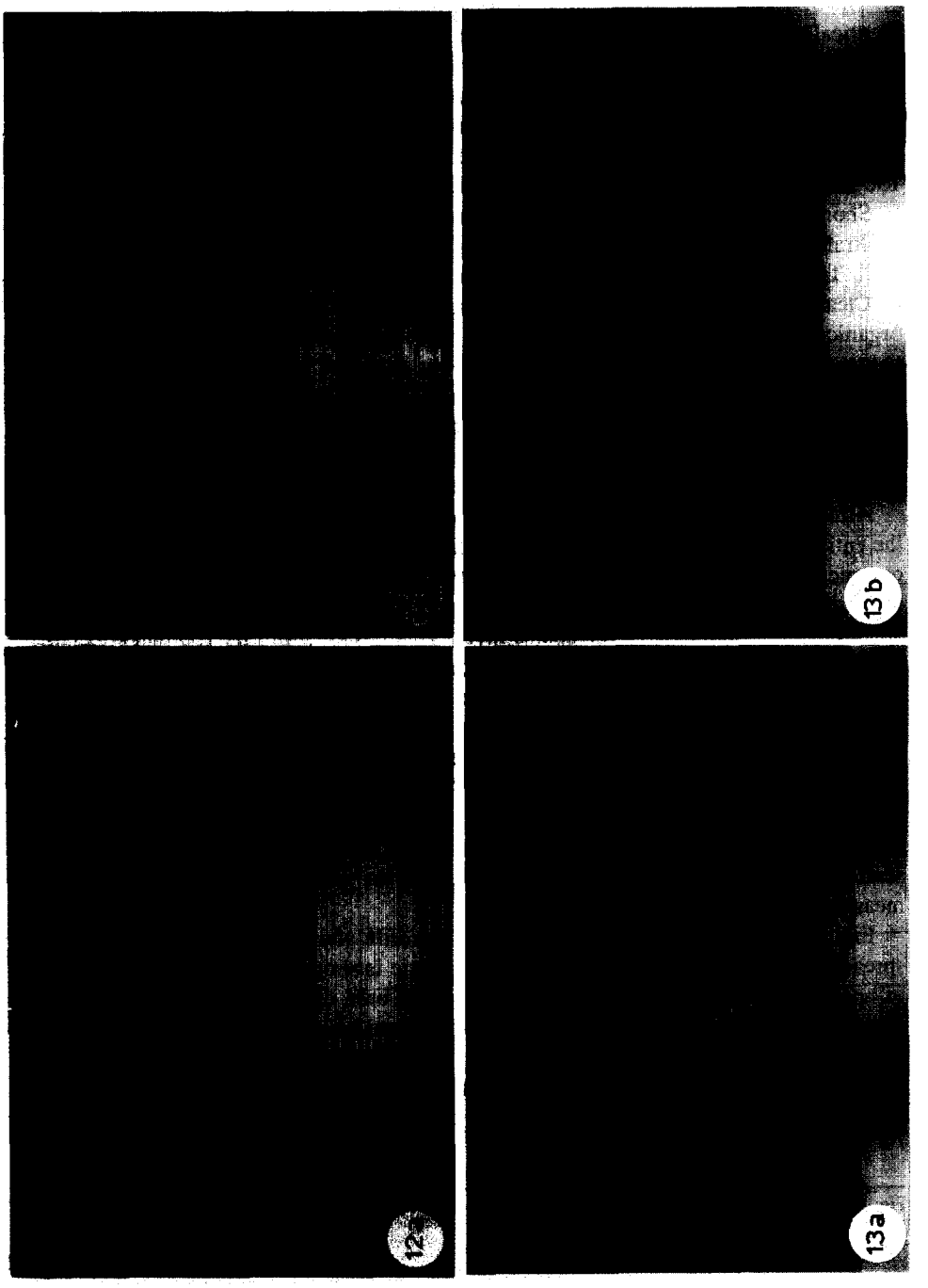

Figs. 12a, b and 13a, b. For the caption to Fig. 12a and b, see p. 19; for the caption to Fig. 13a and b, see p. 22.

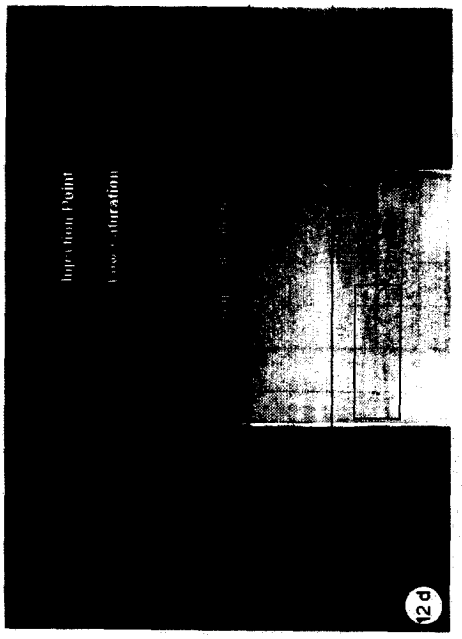

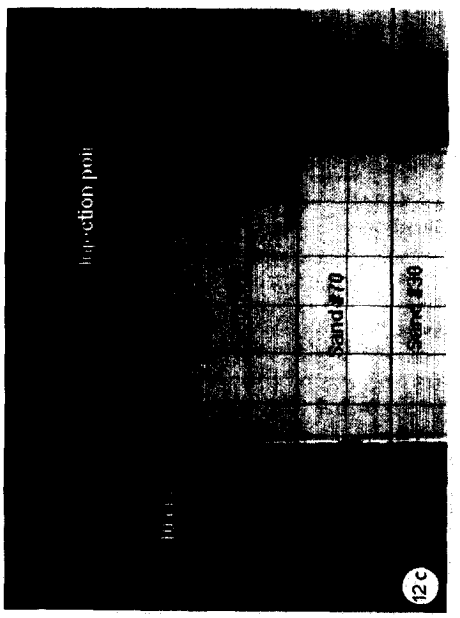

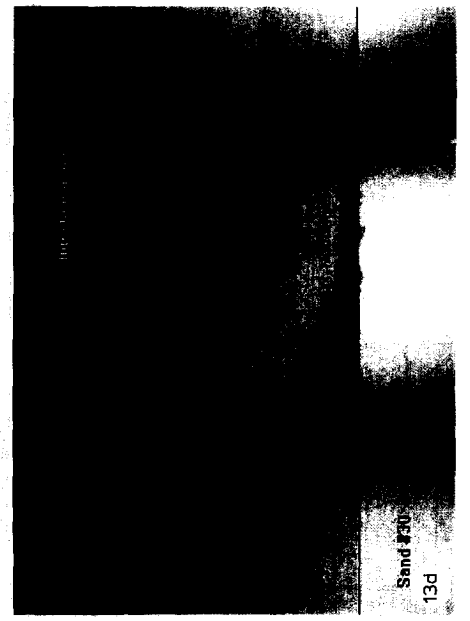

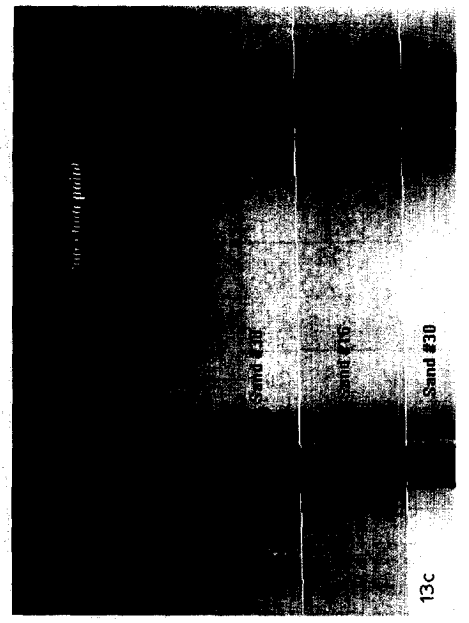

Figs. 12c, d and 13c, d. For the caption to Fig. 12c and d, see p. 19; for the caption to Fig. 13c and d, see p. 22.

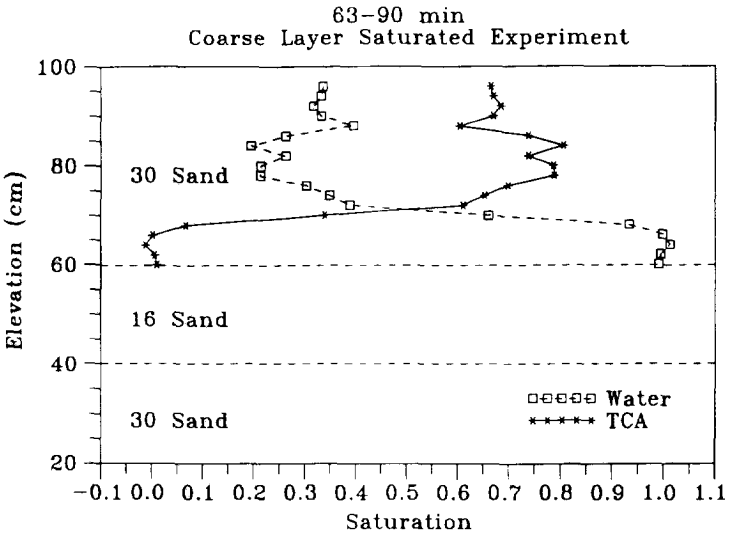

Fig. 14. Saturation profiles of coarse-layer TCA experiment 63–90 min after spill.

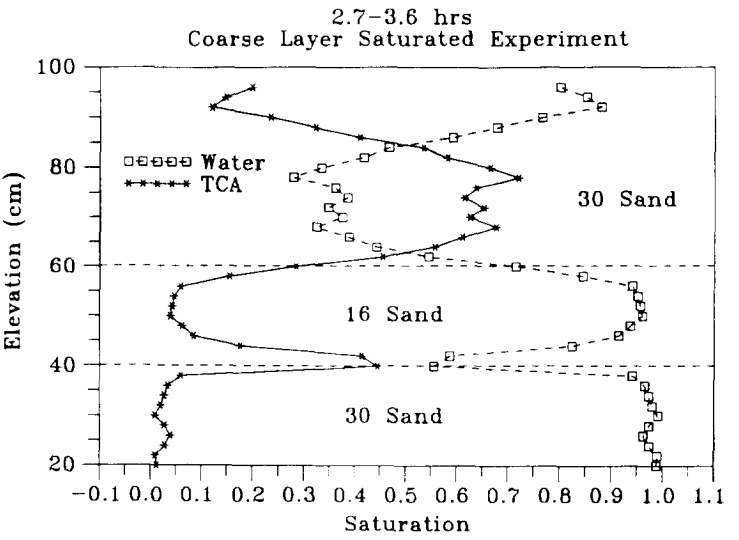

Fig. 15. Saturation profiles of coarse-layer TCA experiment 2.7–3.6 h after spill.

Fig. 13. Photographs of:
a. Coarse-layer experiment, 30 min after spill.
b. Coarse-layer experiment, 2 h after spill.
Ibidem, with captions:
c. Plume configuration, 30 min after the spill in the coarse-layer experiment.
d. Plume configuration, 2 h after the spill in the coarse-layer experiment.

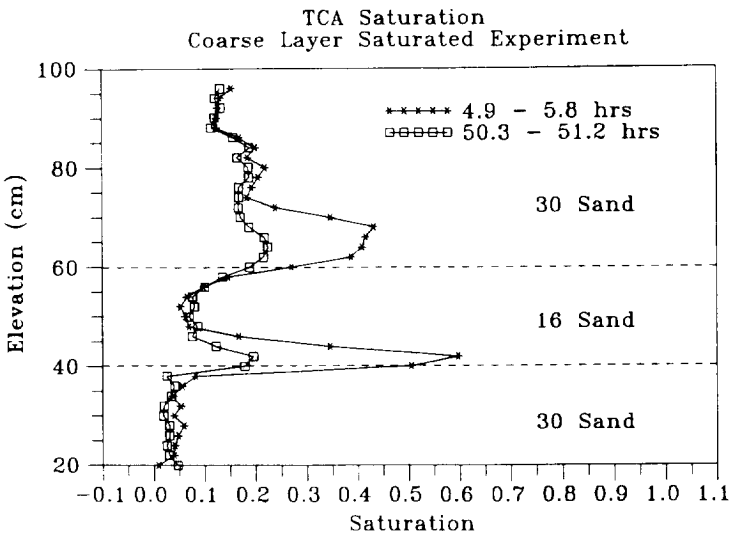

Fig. 16. Saturation profiles of coarse-layer TCA experiment 4.9– 51.2 h after spill.

TCA saturation data in the unstable flow areas do not represent the saturation of the fingers themselves, but do represent the macroscopic saturation. TCA saturations above 5% occurred at several locations where visual inspection of the flume indicated the organic was not present.

4. Conclusions

The laboratory simulation demonstrates the importance of soil heterogeneities in the transport and entrapment behavior of dense nonaqueous-phase organic chemicals. The qualitative and quantitative data collected during the spills will be useful in the validation of numerical models. A number of observations were made which have implications on the understanding of the fundamental processes, developing modeling strategies and designing field characterization techniques. Only a summary of the experimental results were presented in this paper. Additional data on soil packing configurations, boundary conditions, spill conditions and saturation profiles are found in Ramsey (1992).

One of the principal observations was that the initial water saturation has a major impact on the transport of the organic. In the unsaturated zone, the capillary forces of fine soil pulls the contaminant from the coarse soil and entraps it. However, in the saturated zone, the same fine soil established a capillary barrier to the organic phase.

Soil layering was found to significantly increase the spreading of these immiscible contaminants in both the water-saturated and unsaturated regions. The maximum amount of spreading was observed at the first occurrence of a coarse layer overlying a fine layer.

The organic infiltration rate and the contrast in permeability between the soils affect the degree of spreading

In the unsaturated zone, capillary forces of the fine soil entrapped the majority of the organic. Of the organic that did reach the capillary fringe, none was able to achieve the entry pressure necessary to penetrate the water table. This observation was somewhat surprising in the TCA experiments because of the high density of the organic. It is possible that fluctuations of the water table may aid the organic in penetrating the saturated zone. Also, unstable flow phenomena were not observed in the unsaturated region.

In contrast, TCA transport through water-saturated porus media was very unstable. Stable flow occurred during the injection of the organic as a constant head was applied to the organic phase. Soon after the injection discontinued, unstable flow developed. Because the size of the resulting fingers was much smaller than the thickness of the flume we were unable to observe the number of fingers or the frequency of occurrence.

Acknowledgements

This research was supported by the U.S. Environmental Protection Agency through the Great Plains–Rocky Mountain Hazardous Substance Research Center at Kansas State University, Manhattan, Kansas. The authors also acknowledge the support of the Danish Research Academy and the Groundwater Center at the Technical University of Denmark

References

Abriola, L.M. and Pinder, G.F., 1985. A multiphase approach to the modeling of porous media contamination by organic compounds, 1. Equation development. Water Resour. Res., 21(1): 11–18.

Al-Sheriadeh, M. and Illangasekare, T.H., 1993. Efficient immiscible multiphase flow model for heterogeneous porous media. Proc. Conf. on Groundwater Modeling, IGWMC (Int. Ground Water Model. Cent.), Colorado School of Mines, Golden, CO, June 1993, pp. 3-10–3-19.

Buckley, S.E. and Leverett, M.C., 1942. Mechanism of fluid displacement in sands. Trans. Am. Min. Metall. Pet. Eng., 146: 107–116.

Butts, M.B., Jensen, K.H., Szlag, D. and Illangasekare, T.H., 1993. Fate of the miscible and immiscible compounds following a light oil spill. Proc. Conf. on Groundwater Modeling, IGWMC (Int. Ground Water Model. Cent.), Colorado School of Mines, Golden, CO, June 1993, pp. 3-1–3-9.

Campbell, J.H., 1992. Nonaqueous phase liquid flow through porous media: experimental study and conceptual sharp-front model development. M.S. Thesis, Department of Civil, Environmental and Architectural Engineering, University of Colorado, Boulder, CO, 179 pp.

Faust, C.R., Guswa, J.H. and Mercer, J.W., 1989. Simulation of three-dimensional flow of immiscible fluids within and below the unsaturated zone. Water Resour. Res., 25(12): 2449–2464.

Glass, R.J., Parlange, Y-J. and Steenhuis, T.S., 1989. Wetting front instability, 1. Theoretical discussion on dimensional analysis. Water Resour. Res., 25(6): 1195–1207

Held, R. and Illangasekare, T.H., 1995a. Fingering of dense nonaqueous phase liquids in porous media, 1. Experimental investigation. Water Resour. Res., 31(5): 1213–1222.

Held, R. and Illangasekare, T.H., 1995b. Fingering of dense nonaqueous phase liquids in porous media, 2. Analysis and classification. Water Res. Resour., 31(5): 1223–1231.

Hill, D.E. and Parlange, Y-J., 1972. Wetting front instability in layered soil. Soil Sci. Soc. Am. Proc., 36: 697–702.

Illangasekare, T.H., Znidarcic, D., Walser, G. and Weaver, J., 1994. An experimental evaluation of two sharp front models for vadose zone non-aqueous phase liquid transport. Robert S. Kerr Environ. Res. Lab., Ada, OK, Environ. Prot. Agency Rep. EPA/600/R-94/197, 185 pp.

Kaluarachchi, J.J. and Parker, J.C., 1989. An efficient finite element method for modeling of multiphase flow. Water Resour. Res., 25(10): 43–54.

Kueper, B.H. and Frind, E.O., 1991. Two-phase flow in heterogeneous porous media, 1. Model development. Water Resour. Res., 27(6): 1049–1057.

Manna, M., 1991. Suction–saturation measurements in soils using the flow pump technique. M.S. Thesis, Department of Civil, Environmental and Architectural Engineering, University of Colorado, Boulder, CO, 71 pp.

McWhorter, D.B. and Sunada, D.K., 1990. Exact integral solutions for two-phase flow. Water Resour. Res., 26(3): 399–414.

Nofziger, D.L. and Swartzendruber, D., 1974. Material content of binary physical mixtures as measured with dual-gamma beam of gamma rays. J. Appl. Phys., 45(12): 5443–5449.

Peters, E.J. and Flock, D.L., 1981. The onset of instability during two phase immiscible displacement in porous media. Soc. Pet. Eng. J., 21: 249–258.

Ramsey, J.L., 1992. Experimental investigation of dense organic contaminant transport through heterogeneous porous media. M.S. Thesis, Department of Civil, Environmental and Architectural Engineering, University of Colorado, Boulder, CO, 91 pp.

Ryan, P.A. and Cohen, Y., 1991. One dimensional subsurface transport of a nonaqueous phase liquid containing sparingly water soluble organics: a front tracking model. Water Resour. Res., 27(7): 1487–1500.

Schwille, F., 1988. Dense Chlorinated Solvents in Porous and Fractured Media. Lewis, Chelsea, MI.

Stokes, J.P., Weitz, D.A., Gollub, J.P., Dougherty, A., Robbins, M.O., Chaikin, P.M. and Lindsay, H.M., 1986. Interfacial stability of immiscible displacement in a porous medium. Phys. Rev. Lett., 57(4): 1718–1721.

Walser, G.S., Illangasekare, T.H. and Corey, A.T., 1994. Retention of liquid contaminants in layered soils. Proc. 9th Annu. Conf. on Hazardous Waste Remediation, Montana State Univ., Bozeman, MT, June 8–10, 1994, pp. 35–48.